

SparseWorld-TC: Trajectory-Conditioned Sparse Occupancy World Model

Jiayuan Du^{1,2*}, Yiming Zhao^{2*}, Zhenglong Guo², Yong Pan², Wenbo Hou², Zhihui Hao²,
Kun Zhan², Qijun Chen^{1†}

¹Tongji University, ²Li Auto Inc.

Abstract

This paper introduces a novel architecture for trajectory-conditioned forecasting of future 3D scene occupancy. In contrast to methods that rely on variational autoencoders (VAEs) to generate discrete occupancy tokens, which inherently limit representational capacity, our approach predicts multi-frame future occupancy in an end-to-end manner directly from raw image features. Inspired by the success of attention-based transformer architectures in foundational vision and language models such as GPT and VGGT, we employ a sparse occupancy representation that bypasses the intermediate bird’s eye view (BEV) projection and its explicit geometric priors. This design allows the transformer to capture spatiotemporal dependencies more effectively. By avoiding both the finite-capacity constraint of discrete tokenization and the structural limitations of BEV representations, our method achieves state-of-the-art performance on the nuScenes benchmark for 1–3 second occupancy forecasting, outperforming existing approaches by a significant margin. Furthermore, it demonstrates robust scene dynamics understanding, consistently delivering high accuracy under arbitrary future trajectory conditioning. Code: <https://github.com/MrPicklesGG/SparseWorld>.

1. Introduction

World models offer a principled framework for understanding environmental dynamics and are considered essential for AI systems operating in the physical world. Although the literature has yet to converge on a unified and explicit definition of world models, the ability to predict the evolution of the physical environment is consistently regarded as a core capability [5, 15]. Among recent advances, occupancy-based world models have emerged as a prominent category [7, 22, 31, 36, 40, 47, 53], garnering significant interest due to their direct applicability in autonomous driving and robotics, as well as their role in generating temporally consistent sensor observations [2, 29].

*Equal contribution

†Corresponding author

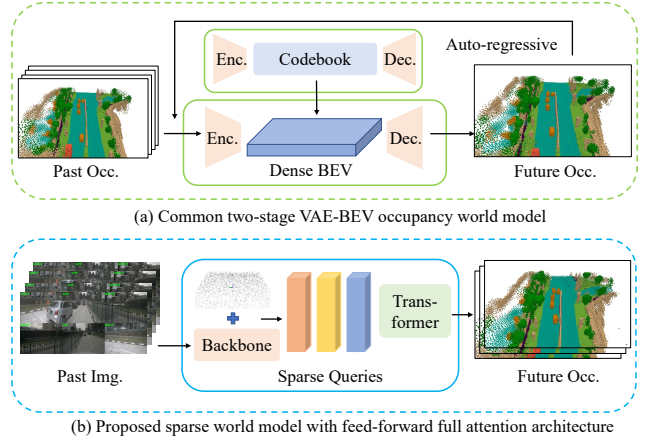


Figure 1. Without VAE codebook and BEV representations, the model represents future multi-frame occupancy using sparse queries and leverages image evidence from prior frames to convert randomly sampled 3D points into reliable future occupancy.

Despite this progress, many recent approaches encode observations into discrete tokens using variational autoencoders (VAEs) [14, 37] and then predict future occupancy from these limited-vocabulary representations [7, 22, 31, 53]. Such tokenization can constrain representational capacity and discard fine-grained information. Alternatively, some methods recast occupancy world modeling as predicting dynamic and static flow fields [43, 51], which does not inherently preserve generative capabilities.

Motivation. Pure attention-based feed-forward architectures have demonstrated remarkable flexibility and representational capacity in both language and 3D vision domains, as exemplified by models such as GPT [1] and VGGT [39]. However, these capabilities remain underexplored for future occupancy prediction. Unlike methods that depend on fixed-resolution bird’s eye view (BEV) representations, which introduce explicit geometric constraints into feature interactions, we propose a pure attention-based transformer architecture that leverages fully sparse occupancy representations to directly capture spatiotemporal relationships from raw image features. Our approach eliminates both discretized tokens and explicit BEV geometric

priors, enabling more effective integration of spatiotemporal dependencies, as illustrated in Figure 1.

Building upon recent advances in sparse perception models [25, 33], we represent scene occupancy using a set of anchors, each composed of a group of 3D query points and an associated feature vector. For each future frame, the anchor features interact through self-attention and cross-attention mechanisms with image features from past frames, accessed via deformable attention. This process iteratively refines the initially randomized points into accurate, context-aware occupancy representations. Trajectory information is incorporated as a conditioning signal to steer the temporal evolution of the predicted scene.

Contribution. We summarize our contributions below:

- We propose a pure attention-based transformer architecture for occupancy world modeling, which integrates spatiotemporal information through sparse occupancy representations in an end-to-end manner, eliminating the need for discrete tokens and bypassing BEV geometric priors.
- We introduce a trajectory-conditioned occupancy forecasting framework that facilitates precise guidance of scene evolution along given trajectories while ensuring high temporal consistency.
- Our method achieves state-of-the-art performance on the nuScenes benchmark [3, 36] for 1–3 second occupancy forecasting and demonstrates compelling results on long-term forecasting benchmarks [7, 31].

2. Related Work

4D occupancy forecasting, which models spatiotemporal scene occupancy (3D space + 1D time) from historical observations, serves as a core foundation for autonomous driving. Recent advances in this area can be categorized along three key technical dimensions: tokenization strategy, intermediate representation, and generation paradigm.

For **tokenization strategies**, existing works [7, 8, 11, 22, 31, 40, 44, 47, 48, 53] mainly adopt VAE [14] or VQ-VAE [37] based approaches. OccWorld [53] utilizes an occupancy VQ-VAE to discretize continuous 3D scene data into discrete tokens. OccLLaMA [44] extends this direction with a VAE-like scene tokenizer optimized for the sparsity and class imbalance of semantic occupancy, enabling unified visual-language-action modeling. RenderWorld [48] introduces AM-VAE, a dual-codebook variant of VQ-VAE that separately encodes air and non-air voxels to enhance the granularity of the representation. I²-World [22] further advances VAE-based tokenization by designing a multi-scale architecture, which refines token granularity across different spatial scales to capture both local details and global scene structures. In contrast, DOME [7] and COME [31] employ a continuous Occ-VAE instead of discrete tokenization, preserving fine-grained details through

continuous latent spaces.

Intermediate representations must balance precision and efficiency, including BEV feature [4, 7, 11, 17, 22, 31, 46, 51, 53], Gaussian representation [48, 54], and others like triplane [45] or hexplane [2]. Most VAE-based methods [7, 11, 22, 31, 44, 53] rely on dense BEV feature maps for spatial-temporal modeling and conditional scene generation. PreWorld [17] validates BEV’s effectiveness through pre-training, while DFIT-OccWorld [51] uses it for flow prediction. GaussianAD [54] and RenderWorld [48] adopt 3D Gaussian splatting [12] to model scenes as anisotropic Gaussian ellipsoids, achieving efficient rendering and high segmentation accuracy. DTT [45] and DynamicCity [2] utilize triplane or hexplane as intermediate representations, which retain 3D structural information while achieving more compact latent spaces.

Regarding **generation paradigms**, autoregressive modeling [11, 17, 22, 44, 47–49, 53] remains prevalent for sequential scene prediction, though non-autoregressive [51] and diffusion-based [7, 31, 45] alternatives have gained traction. OccWorld [53] and RenderWorld [48] use hierarchical transformers for autoregressive future scene token prediction. OccLLaMA [44] and Occ-LLM [47] leverage large language models to perform cross-modal next-token/scene autoregressive modeling. DFIT-OccWorld [51] stands out by adopting a non-autoregressive paradigm based on its BEV intermediate representations, which accelerates generation speed compared to autoregressive counterparts while maintaining scene integrity. DOME [7] leverages a spatial-temporal diffusion transformer, and COME [31] extends this diffusion framework with ControlNet [52] to enable conditional diffusion-based generation.

Proposed Method. Rather than relying on handcrafted tokenizers or intermediate representations, our approach prefers to model the occupancy-based world in an end-to-end manner. Scenes are represented as sets of learnable feature embeddings, with their interactions mediated by attention mechanisms. This formulation departs from diffusion-based and autoregressive paradigms, favoring a VGGT-like feed-forward architecture [39] that predicts future occupancy in a single forward pass. Under this design, conditioning scene evolution on a given trajectory is straightforward: we embed the trajectory as feature vectors and let them interact with the scene features.

3. Methodology

3.1. Sparse World Model Representation

Most existing approaches model 3D scene occupancy using dense voxel grids [18], which are typically constructed on BEV representations. Although effective, such BEV-based paradigms impose explicit geometric constraints that can limit the flexible interaction of spatiotemporal features

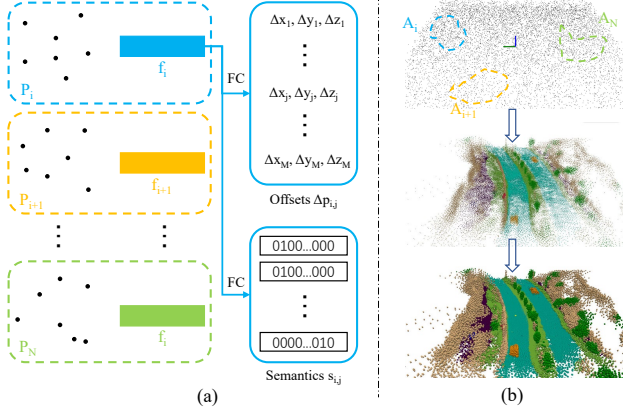


Figure 2. Occupancy is modeled as a collection of anchors formed by a bundle of 3D points paired with an occupancy embedding. The embedding is decoded by two MLPs to yield per point offsets and semantic class logits, which denoise sampled points to a consistent occupancy field.

across different scales. Inspired by recent advances in sparse perception models that bypass BEV as an intermediate representation [24–26, 38], we propose an alternative occupancy formulation based on a collection of anchors. In our framework, each anchor consists of a set of randomly initialized 3D points and an associated feature vector that jointly predicts per-point geometric offsets and semantic labels, as illustrated in Figure 2. Based on this sparse occupancy representation, we define the world model as a sequence of such single-frame occupancy states conditioned on a given trajectory.

Single Frame Occupancy Representation. We represent the initial occupancy of a single frame by \mathcal{M} , which comprises N anchors, each associated with a feature vector:

$$\mathcal{M} = \{A_i\}_{i=1}^N, \quad A_i = (P_i, \mathbf{f}_i) \quad (1)$$

where $P_i = \{\mathbf{p}_{i,j} \in \mathbb{R}^3\}_{j=1}^M$ denotes a set of M 3D points for anchor i , and $\mathbf{f}_i \in \mathbb{R}^D$ is the corresponding feature vector. The feature vector \mathbf{f}_i predicts for each point $\mathbf{p}_{i,j}$ both an offset $\Delta \mathbf{p}_{i,j} \in \mathbb{R}^3$ and a semantic label $\mathbf{s}_{i,j} \in \mathbb{R}^C$ (a C -dimensional class probability vector). The representation \mathcal{M} is initialized as follows: the centers $\{\mathbf{c}_i\}_{i=1}^N$ are uniformly distributed in the 3D space, $\mathbf{c}_i \sim \mathcal{U}(\text{Space})$; each set of points P_i is randomly initialized within a local region around \mathbf{c}_i as $\mathbf{p}_{i,j} \leftarrow \mathbf{c}_i + \epsilon_{i,j}$ with $\epsilon_{i,j} \sim \mathcal{N}(\mathbf{0}, \sigma^2 \mathbf{I})$; and all feature vectors are initialized to zero, $\mathbf{f}_i \leftarrow \mathbf{0}$.

Trajectory Representation. In autonomous driving, the planned future trajectory of the ego vehicle provides an essential conditioning signal for predictive world modeling. We parameterize a future trajectory τ as a sequence of discrete states spanning a temporal horizon T :

$$\tau = \{\mathbf{x}_t\}_{t=1}^T \quad (2)$$

Each state $\mathbf{x}_t \in \mathbb{R}^d$ encapsulates the ego’s kinematic status at time t . In our formulation, each state comprises the vehicle’s planar position (x, y) , its heading angle θ , and the timestamp t itself, providing a compact yet expressive representation for conditioning the world model.

World Model Representation. The world model \mathcal{F} synthesizes future scene evolution conditioned on the planned trajectory and historical observation. Formally, the model generates a sequence of future occupancy states:

$$\mathcal{O}_{1:T} = \mathcal{F}(\mathcal{M}_{1:T}, \mathbf{S}_{-T':0}, \tau) \quad (3)$$

where $\mathcal{M}_{1:T}$ denotes the initial state representation of all future frames, $\mathbf{S}_{-T':0}$ represents a history of sensor observations from the past T' timesteps, and τ is the given trajectory. This formulation enables the model to integrate past context and future intentions to render physically consistent future scenes, thereby supporting downstream tasks such as motion planning and predictive safety assessment. Since the anchor points in $\mathcal{M}_{1:T}$ are stochastically initialized, our occupancy world model operates similarly to a conditional video generation model that transforms random 3D point clouds into sequential driving scenarios conditioned on both past sensor observations and future trajectory information.

3.2. Spatial Temporal Fusion Architecture

In Equation 1, the occupancy of the scene is represented by a set of feature vectors. We further embed both the trajectory waypoints and the historical sensor observations into separate feature representations. Once all modalities are projected into a unified embedding space, they can be efficiently fused and interact through attention mechanisms within our proposed pure attention-based architecture.

3.2.1. Trajectory Spatiotemporal Embedding

As mentioned above, our trajectory representation incorporates the position and timestamp of each waypoint. To maintain flexibility, we do not assume uniform temporal sampling between waypoints. Instead, we directly embed the individual position and timestamp of each waypoint to accommodate various potential planning outputs.

Position Embedding. In trajectory representation, position embedding captures the spatial characteristics of trajectories by integrating the spatial information of each waypoint into the feature system. Specifically, the 3D coordinates of waypoints first undergo a relative pose transformation for subsequent fusion, then are mapped to the target feature dimension via a multilayer perceptron (MLP). The homogeneous matrix of the relative pose transformation is also mapped to the feature dimension using an MLP, ultimately equipping the features with spatial attributes and ego trajectory information to support subsequent trajectory-conditioned occupancy forecasting.

Time Embedding. Time embedding captures the relative

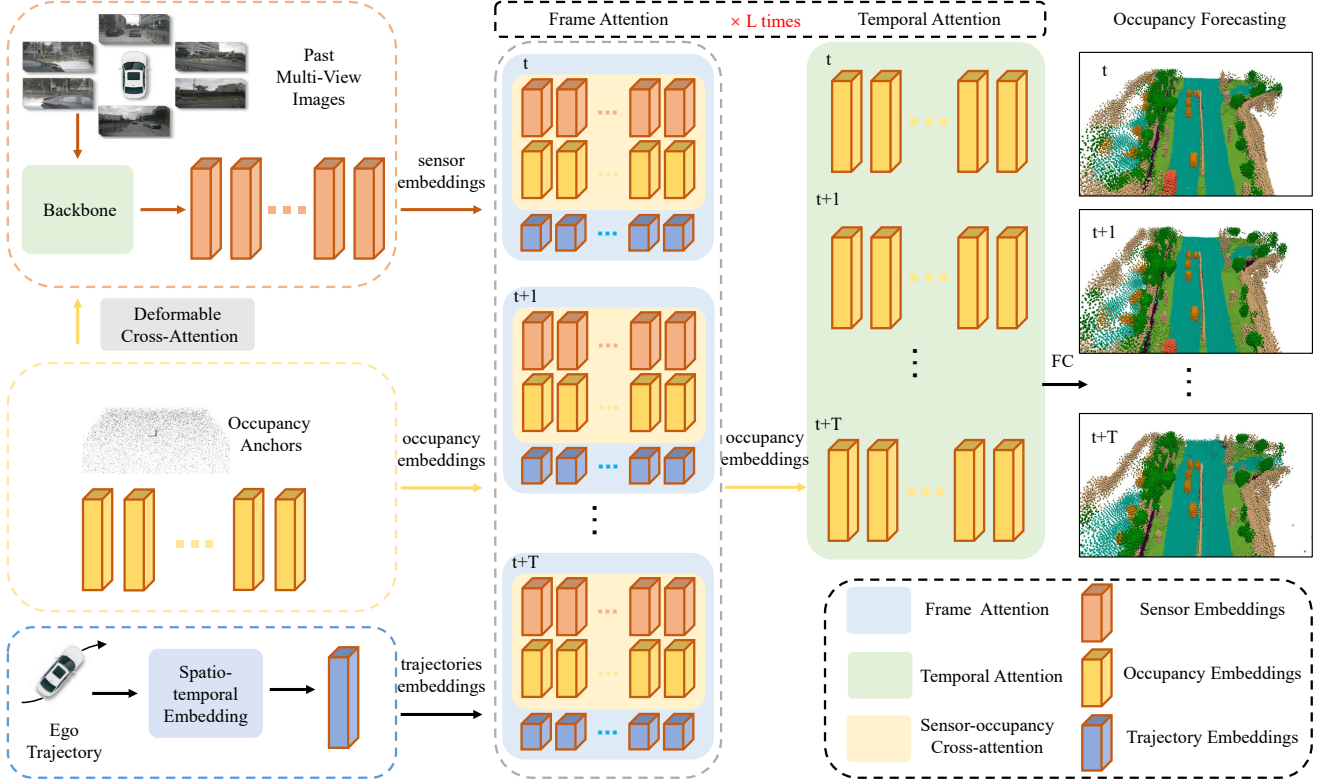


Figure 3. We embed the sensor observations, occupancy priors, and trajectories into feature vectors. These embeddings pass through stacked frame-level attention and temporal attention blocks that iteratively fuse cross-modal and cross-time information into occupancy features. Those occupancy features finally decode random points into meaningful occupancy predictions.

temporal positional relationship of trajectories using a list of future timestamps (e.g. [0, 2, 4, 6]), where "0" denotes the current frame timestamp and other values represent the number of frames relative to the current frame. Classic sine-cosine encoding is employed to embed this relative temporal relationship into the corresponding features.

Spatiotemporal Embedding. Drawing inspiration from motion-aware layer normalization (MLN) [41], spatiotemporal embedding achieves the fusion of spatial and temporal information by building on the aforementioned position embedding and time embedding. Specifically, two linear layers are designed to implicitly learn the affine transformations between adjacent frames. This learning process relies on the spatial attribute cues provided by position embedding and the relative temporal relationship information captured by time embedding, enabling the affine transformations to adapt dynamically to the spatiotemporal characteristics of the trajectory. Subsequently, the implicitly learned affine transformations are applied to the query features: by adjusting the query features through these transformations, the spatial information and temporal information are organically integrated into the query features. The final trajectory τ is thus represented as a set of spatiotemporal feature vectors $\tau = \{\mathbf{f}_t''\}_{t=1}^T$, where \mathbf{f}_t'' denotes the spatiotemporal

feature embedding corresponding to the t frame.

3.2.2. Sensor Embedding with Deformable Attention

Deformable attention is widely used in 3D sparse perception [19, 24, 25, 33, 42]. It projects 3D query points into multi-view image feature maps (and 3D LiDAR voxel grids when LiDAR is available) using known calibration and ego-motion, and samples features at the projected locations.

In our architecture, we take into account m sensors per frame, the center \mathbf{c}_i of each anchor point set P_i serves as the query point in the deformable attention operation, where we calculate the mean and standard deviation of anchor point set P_i along the x, y, z directions as the basis for sampling offsets. Each center is projected into the multi-scale image feature maps of the backbone (e.g. ResNet [9] or ViT [6]) using camera intrinsics, extrinsics and the ego pose. If a query projects into multiple views due to field-of-view overlap, we aggregate by averaging the sampled features across all m views. Each anchor center collects features from the past T' frames. To encode temporal context, we add a sinusoidal time embedding processed by a fully connected layer to provide motion cues. Finally, for each future frame with occupancy representation \mathcal{M} , we obtain the sensor embedding representation $\mathcal{S} = \{\mathbf{f}_i'\}_{i=1}^{N \times T'}$.

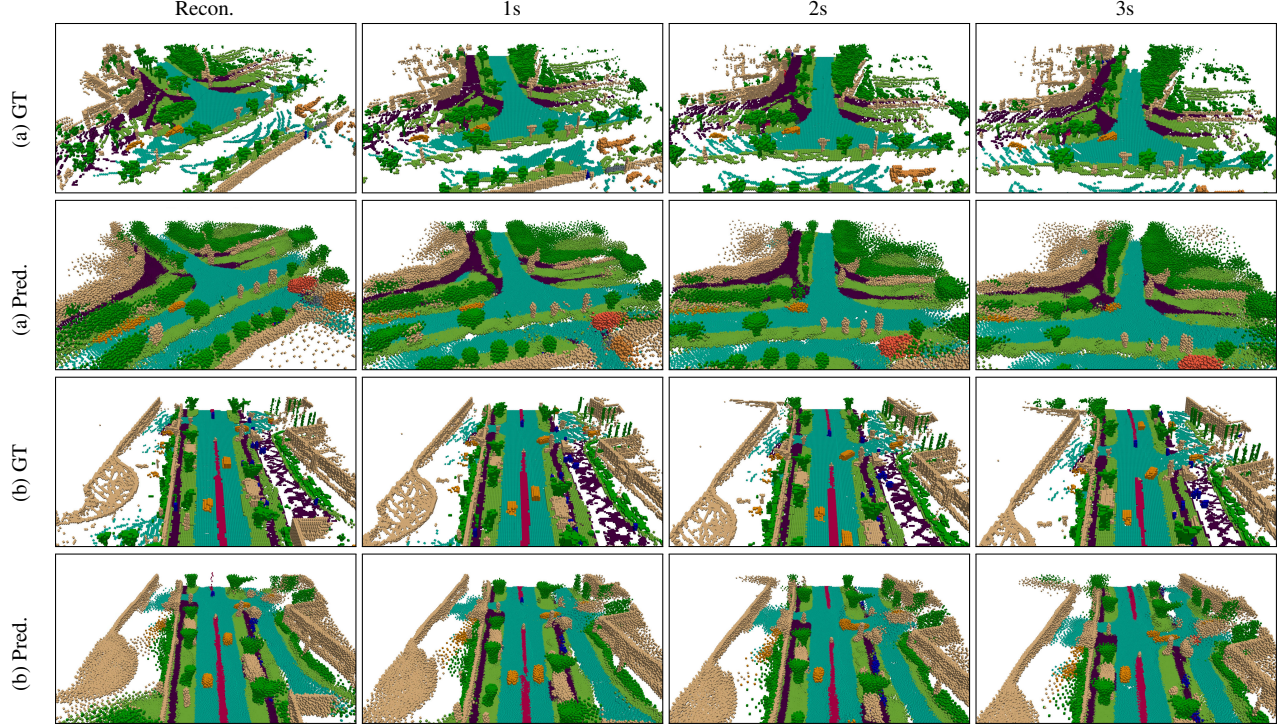


Figure 4. Qualitative results of our proposed SparseWorld-TC are presented here. Our method effectively captures both dynamic and static changes in the surrounding environment over a 3-second forecasting horizon.

3.2.3. Fully Attention Fusion Architecture

In Equation 3, $\mathcal{F}(\cdot)$ denotes the neural network architecture to be designed. In our approach, the world occupancy representation $\mathcal{M}_{1:T}$, the sensor representation $\mathbf{S}_{-T':0}$, and the trajectory representation τ are all projected into a unified embedding space. Accordingly, the world model can be reformulated as:

$$\mathcal{O}_{1:T} = \mathcal{F}\left(\{\mathbf{f}_i\}_{i=1}^{N \times T}, \{\mathbf{f}'_i\}_{i=1}^{N \times T \times T'}, \{\mathbf{f}''_t\}_{t=1}^T\right) \quad (4)$$

Note that the point sets P_i in Equation 1 consist of non-learnable random coordinates and are therefore omitted from the input in Equation 4.

Equation 4 provides a compact formulation of our world model: all relevant features interact directly via standard attention. We employ a feed-forward, purely attention-based transformer architecture, shown in Figure 3. For each future frame t , the occupancy embeddings $\{\mathbf{f}_i^t\}_{i=1}^N$ attend to the past sensor embeddings $\{\mathbf{f}'_{ij}\}_{i=1}^{N \times T'}$ via cross-attention. The updated occupancy features are then fused with the trajectory embedding through frame-level self-attention. Finally, a temporal attention block applies self-attention across all future frames, jointly refining the set of occupancy embeddings $\{\mathbf{f}_i\}_{i=1}^{N \times T}$ to capture longer-range spatiotemporal dependencies. We stack the frame and temporal attention modules and apply them for multiple iterations, progres-

sively refining the randomly initialized 3D anchor points into accurate occupancy predictions over the next T frames.

3.3. Training Strategies

While the nuScenes occupancy world-model benchmark evaluates forecasting horizons of 1–3 seconds, some studies consider much longer futures (e.g., up to 10 seconds). This motivates us to design a flexible model that adapts to diverse forecasting requirements, supporting future occupancy prediction over arbitrary horizons and even at varying time intervals. We achieve this through a random ensemble strategy that enhances the generalization capability of the trained model without modifying the network architecture.

Random Ensemble Strategy. We assume a maximum forecasting horizon T . During training, we randomly choose a target sequence length L , where $L \in \{2, \dots, T\}$, and supervise the model with the corresponding L future occupancy frames. Because no fixed temporal stride is prescribed, the scene evolution is governed solely by the trajectory embeddings, which encode temporal and positional context. This flexible supervision scheme enables the model to adapt to diverse forecasting requirements and improves overall performance, as shown in our ablation studies.

Loss Term. We extract the center of each ground-truth occupancy voxel as target points and optimize the Chamfer Distance loss \mathcal{L}_{CD} (Equation 5) to align the predicted

Table 1. 4D occupancy forecasting performance on Occ3D-nuScenes [36]. Input denotes the modality of input apart from the ego trajectory. Avg. denotes average performance of that in 1s, 2s, and 3s.

Method	Input	Semantic mIoU (%) \uparrow				Geometric IoU (%) \uparrow				FPS \uparrow
		1s	2s	3s	Avg.	1s	2s	3s	Avg.	
OccWorld-O [53]	Occ GT	25.78	15.14	10.51	17.14	34.63	25.07	20.18	26.63	18.00
OccLLaMA-O [44]	Occ GT	25.05	19.49	15.26	19.93	34.56	28.53	24.41	29.17	-
RenderWorld [48]	Occ GT	28.69	18.89	14.83	20.89	37.74	28.41	24.08	30.08	-
Occ-LLM [47]	Occ GT	24.02	21.65	17.29	20.99	36.65	32.14	28.77	35.52	-
DFIT-OccWorld [51]	Occ GT	31.68	21.29	15.19	22.71	40.28	31.24	25.29	32.27	-
DOME [7]	Occ GT	35.11	25.89	20.29	27.10	43.99	35.36	29.74	36.36	6.54
UniScene [16]	Occ GT	35.37	29.59	25.08	31.76	38.34	32.70	29.09	34.84	-
I ² -World [22]	Occ GT	47.62	38.58	32.98	39.73	54.29	49.43	45.69	49.80	37.04
RenderWorld [48]	Camera	2.83	2.55	2.37	2.58	14.61	13.61	12.98	13.73	-
OccWorld-D [53]	Camera	11.55	8.10	6.22	8.62	18.90	16.26	14.43	16.53	-
OccLLaMA [44]	Camera	10.34	8.66	6.98	8.66	25.81	23.19	19.97	22.99	-
PreWorld [17]	Camera	12.27	9.24	7.15	9.55	23.62	21.62	19.63	21.62	-
Occ-LLM [47]	Camera	11.28	10.21	9.13	10.21	27.11	24.07	20.19	23.79	-
DFIT-OccWorld [51]	Camera	13.38	10.16	7.96	10.50	19.18	16.85	25.02	17.02	-
OccVAR [11]	Camera	17.17	10.38	7.82	11.79	27.60	25.14	20.33	24.35	-
DOME-STC [7]	Camera	17.79	14.23	11.58	14.53	26.39	23.20	20.42	23.33	2.75
I ² -World-STC [22]	Camera	21.67	18.78	16.47	18.97	30.55	28.76	26.99	28.77	4.21
DOME-F [7]	Camera	24.12	17.41	13.24	18.25	35.18	27.90	23.44	28.84	-
DTT [45]	Camera	24.87	18.30	15.63	19.60	38.98	37.45	31.89	36.11	-
COME-F [31]	Camera	26.56	21.73	18.49	22.26	48.08	43.84	40.28	44.07	-
SparseWorld-TC-Small (Ours)	Camera	27.95	25.51	23.35	25.60	50.69	49.15	47.23	49.02	9.35
SparseWorld-TC-Large (Ours)	Camera	28.64	26.28	24.36	26.42	50.57	49.26	47.80	49.21	3.58
SparseWorld-TC-Small* (Ours)	Camera	30.09	27.61	25.43	27.71	52.66	51.20	49.31	51.05	5.63
SparseWorld-TC-Large* (Ours)	Camera	32.76	29.62	27.28	29.89	55.28	53.56	51.71	53.52	2.08

point distribution with the target points. This loss function is widely adopted in point cloud processing [13, 50] and occupancy modeling [38], as it effectively measures the similarity between predicted point clouds \mathbb{P} and target point clouds \mathbb{P}_g . This loss thereby supervises the predicted off-sets, guiding the initially randomized points toward the precise underlying geometry.

$$\mathcal{L}_{CD} = \frac{1}{|\mathbb{P}|} \sum_{\mathbf{p} \in \mathbb{P}} D(\mathbf{p}, \mathbb{P}_g) + \frac{1}{|\mathbb{P}_g|} \sum_{\mathbf{p}_g \in \mathbb{P}_g} D(\mathbf{p}_g, \mathbb{P}), \quad (5)$$

where $D(\mathbf{x}, \mathbb{Y}) = \min_{\mathbf{y} \in \mathbb{Y}} \|\mathbf{x} - \mathbf{y}\|_1$. Following [38], the matched target point also provides a semantic label. Consequently, we supervise semantic predictions using the standard focal classification loss \mathcal{L}_{focal} [23], which yields the overall objective:

$$\mathcal{L} = \mathcal{L}_{CD} + \mathcal{L}_{focal}. \quad (6)$$

4. Experiments

4.1. Experimental Setup

Dataset and Metrics. Experiments are conducted on the widely adopted Occ3D-nuScenes benchmark [36]. Our implementation strictly follows the experimental settings established in previous works [7, 22, 31, 47, 51, 53]. For evaluation, we adopt the standard geometric Intersection over Union (IoU) and semantic mean Intersection over Union (mIoU) metrics.

Implementation Details. As detailed in the methodology section, our architecture includes several configurable components. We pick past frames within the past 2 seconds, following recent models [7, 22, 31, 47, 51, 53]. The future prediction horizon T is set to 3s and 8s, aligning with established benchmarks [7, 53]. To accommodate varying computational constraints, we configure the number of anchors per frame as $N = 600$, with each anchor comprising $M = 128$ points. This configuration, designated as SparseWorld-TC-Small, adopts a ResNet-50 backbone [9]. Our SparseWorld-TC-Large variant uses $N = 4800$ and

Table 2. Long-term 4D occupancy forecasting performance.

Method	Input	Semantic mIoU (%) \uparrow								
		1s	2s	3s	4s	5s	6s	7s	8s	Avg.
DOME [7]	Occ GT	30.10	21.35	17.36	14.86	12.61	11.03	10.00	9.34	15.83
COME [31]	Occ GT	33.78	24.57	21.35	18.25	15.84	13.85	12.99	11.96	19.07
SparseWorld-TC-Large	Camera	28.64	26.28	24.36	22.65	21.07	19.73	18.52	17.42	22.33
Method	Input	Geometric IoU (%) \uparrow								
		1s	2s	3s	4s	5s	6s	7s	8s	Avg.
DOME [7]	Occ GT	39.04	31.20	27.14	24.73	22.32	20.28	19.05	17.97	25.21
COME [31]	Occ GT	44.20	36.25	32.86	30.03	26.93	24.70	23.30	21.44	29.96
SparseWorld-TC-Large	Camera	50.57	49.26	47.80	46.20	44.57	42.98	41.44	39.97	45.35

$M = 16$, delivering improved performance at increased computational cost. Furthermore, leveraging the representational power of DINOv3 [32], we introduce SparseWorld-TC-Small* and SparseWorld-TC-Large*, which adopts a DINOv3-Base image backbone while retaining the same configurations as “-Small” and “-Large” versions. All models are trained for 70 epochs on 8 NVIDIA H20 GPUs with a total batch size of 8, using the AdamW optimizer [28] with an initial learning rate of 2×10^{-4} and a cosine annealing learning rate schedule [27].

4.2. Main Results

4D Occupancy Forecasting. We evaluate our proposed method following established evaluation protocols [7, 22, 51, 53], as summarized in Table 1. While some VAE-based methods report performance using ground-truth occupancy as input, a requirement sometimes unavailable in real-world scenarios, we include these results for a comprehensive comparison. Since our approach directly consumes camera sensor input rather than precomputed occupancy grids, we primarily compare against camera-based versions of prior methods. Note that OccWorld-D uses predictions from TPVFormer [10]; “-STC” and “-F” indicate models incorporating occupancy results from STCOcc [21] and FB-Occ [18], respectively.

Our SparseWorld-TC-Large achieves significant improvements, outperforming the previous state-of-the-art by 18.7% in mIoU (26.42 vs. 22.26) and 11.7% in IoU (49.21 vs. 44.07). Due to the flexible and variable number of queries, our model exhibits strong scalability. SparseWorld-TC-Small achieves 25.60 mIoU and 49.02 IoU, while being approximately twice as fast as SparseWorld-TC-Large and I²-World [22], thus striking an effective balance between performance and efficiency. The strong performance of the DINO version of our method further demonstrates the scalability in leveraging large-scale foundation models.

Moreover, although Table 1 shows that methods using ground-truth occupancy generally achieve better performance than those processing raw sensor inputs, our camera-

based model remains competitive across several metrics. Specifically, SparseWorld-TC-Large* achieves a higher average mIoU (29.89 vs. 27.10) than DOME [7] and a higher average IoU (53.52 vs. 49.80) compared to I²-World [22], which can be attributed to its reduced decay in long-term occupancy forecasting.

Long-term Forecasting. To evaluate the capability of long-term predictions, we extend the prediction period from 3 seconds to 8 seconds. As shown in Table 2, our method consistently outperforms DOME [7] and COME [31] after 2 seconds for the mIoU metric while having better performance in all timestamps for the IoU metric. In general, our method achieves average mIoU and IoU scores of 22.33 and 45.35, surpassing COME [31] by 17.1% and 51.4%, respectively. It is worth noting that our method uses the camera as input, while the contrast methods use ground truth occupancy as input.

4.3. Ablation Study

Table 3. Ablation study on trajectory. Avg. denotes average performance of mIoU or IoU in 1s, 2s, and 3s.

Trajectory			mIoU (%) \uparrow IoU (%) \uparrow	
w/o Traj.	Pred. Traj.	GT Traj.	Avg.	Avg.
\checkmark			15.44	32.19
	\checkmark		21.57	44.76
		\checkmark	25.60	49.02

Effect of Trajectory. Our model supports the conditioning of arbitrary future trajectories. Through ablation studies, we examine how such trajectory guidance influences model behavior and output quality. As summarized in Table 3, we evaluate performance in three settings based on the SparseWorld-TC-Small model: without trajectory input, with trajectories predicted by BEVPlanner [20], and with ground-truth trajectories. The results demonstrate that our model remains robust even when provided with predicted trajectories, while performance consistently improves with more accurate trajectory estimates.

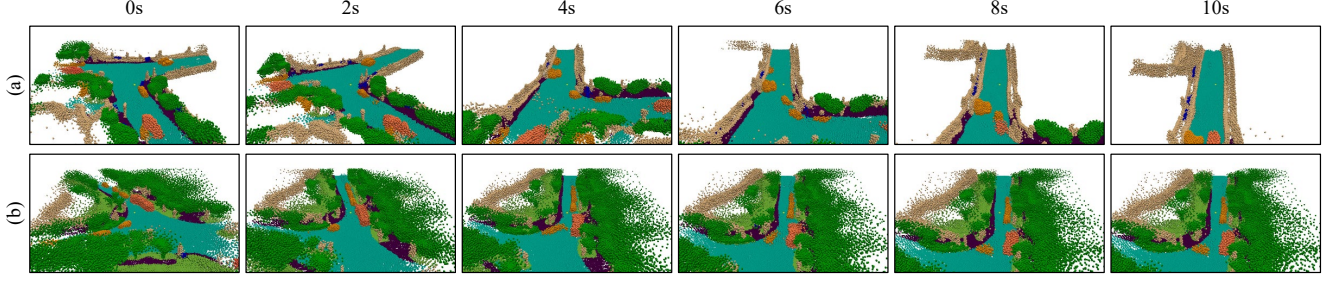


Figure 5. Long-term 4D occupancy world model forecasting.

Table 4. Ablation study on training strategies. Avg. denotes average performance of mIoU or IoU in 1-8s.

Training Strategies		mIoU (%) \uparrow	IoU (%) \uparrow
Fixed	Random Ensemble	Avg.	Avg.
\checkmark		20.36	43.25
	\checkmark	22.33	45.35

Effect of Ensemble Training. We explore the impact of our random ensemble training on the SparseWorld-TC-Large model, as shown in Table 4. In the long-term occupancy forecasting task, the supervision of random future frames is more effective than the supervision of fixed future frames.

4.4. Visualizations & Discussions

4D Occupancy Forecasting. As shown in Figure 4, we provide a visual comparison between our reconstruction results, 1-3 second future predictions, and the corresponding ground truth. Qualitatively, our method demonstrates stable and accurate predictions for static environments while also effectively capturing the motion of dynamic objects. In the left-turn scenario depicted in Figure 4(a), our approach correctly predicts the future occupancy observation of a turning vehicle behind. Similarly, as shown in Figure 4(b), future occupancy predictions for both straight-moving and left-turning vehicles are reliably predicted.

Long-term Forecasting. Figure 5 presents the visualization of our prediction results over a long-term horizon of 10 seconds in two distinct scenarios: (a) a right-turn and (b) a left-turn. Our model maintains strong scene consistency throughout the extended prediction period, with well-preserved geometric structures. The quantitative result is listed in Table 2. Although the intrinsic multi-possibility of long-term forecasting raises questions about the fairness of using a single ground truth for evaluation, we argue that this metric, combined with the visualization results, at least partially demonstrates the potential of our method for relatively long-term occupancy forecasting.

Trajectory-conditioned Forecasting. Figure 6 illustrates that the prediction of future driving scenarios is generated by different trajectories as conditions in a bifurcating road

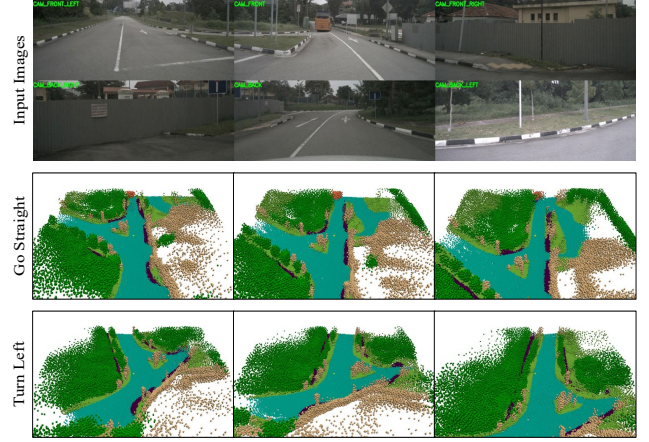


Figure 6. Forecasting with conditioned trajectories.

scenario, embodying the future occupancy prediction capability conditioned by the trajectory of our model.

From Occupancy to Sensors. Building upon the occupancy world model, our proposed architecture is further capable of directly predicting future sensor observations, adopting an extension inspired by [29, 30, 35]. This capability is realized by incorporating additional MLPs into the decoding network illustrated in Figure 2. All of these MLPs collectively generate 3D Gaussian parameters, center offsets, and classification logits in a single feed-forward pass. For a comprehensive exposition of our methodology and additional experimental results, please refer to the supplementary document.

5. Conclusion

We propose a novel trajectory-conditioned architecture for end-to-end 4D occupancy forecasting, which eliminates the need for discrete tokenization or explicit BEV representations. Using fully sparse anchors and a transformer-based fusion mechanism, our model captures spatiotemporal dependencies directly from sensor data, enabling scalable and robust scene prediction. The flexible design supports the integration of alternative 3D representations such as 3D Gaussians, and exploring these alternatives constitutes a promising direction for future work.

References

- [1] Josh Achiam, Steven Adler, Sandhini Agarwal, Lama Ahmad, Ilge Akkaya, Florencia Leoni Aleman, Diogo Almeida, Janko Altenschmidt, Sam Altman, Shyamal Anadkat, et al. Gpt-4 technical report. *arXiv preprint arXiv:2303.08774*, 2023. 1
- [2] Hengwei Bian, Lingdong Kong, Haozhe Xie, Liang Pan, Yu Qiao, and Ziwei Liu. Dynamiccity: Large-scale 4d occupancy generation from dynamic scenes. *arXiv preprint arXiv:2410.18084*, 2024. 1, 2
- [3] Holger Caesar, Varun Bankiti, Alex H Lang, Sourabh Vora, Venice Erin Liong, Qiang Xu, Anush Krishnan, Yu Pan, Giancarlo Baldan, and Oscar Beijbom. nuscenes: A multimodal dataset for autonomous driving. In *CVPR*, pages 11621–11631, 2020. 2
- [4] Junliang Chen, Huaiyuan Xu, Yi Wang, and Lap-Pui Chau. Occprophet: Pushing efficiency frontier of camera-only 4d occupancy forecasting with observer-forecaster-refiner framework. *arXiv preprint arXiv:2502.15180*, 2025. 2
- [5] Jingtao Ding, Yunke Zhang, Yu Shang, Yuheng Zhang, Zefang Zong, Jie Feng, Yuan Yuan, Hongyuan Su, Nian Li, Nicholas Sukiennik, et al. Understanding world or predicting future? a comprehensive survey of world models. *ACM Computing Surveys*, 58(3):1–38, 2025. 1
- [6] Alexey Dosovitskiy. An image is worth 16x16 words: Transformers for image recognition at scale. *arXiv preprint arXiv:2010.11929*, 2020. 4
- [7] Songen Gu, Wei Yin, Bu Jin, Xiaoyang Guo, Junming Wang, Haodong Li, Qian Zhang, and Xiaoxiao Long. Dome: Taming diffusion model into high-fidelity controllable occupancy world model. *arXiv preprint arXiv:2410.10429*, 2024. 1, 2, 6, 7
- [8] Erxin Guo, Pei An, You Yang, Qiong Liu, and An-An Liu. Fsf-net: Enhance 4d occupancy forecasting with coarse bev scene flow for autonomous driving. *arXiv preprint arXiv:2409.15841*, 2024. 2
- [9] Kaiming He, Xiangyu Zhang, Shaoqing Ren, and Jian Sun. Deep residual learning for image recognition. In *CVPR*, pages 770–778, 2016. 4, 6
- [10] Yuanhui Huang, Wenzhao Zheng, Yunpeng Zhang, Jie Zhou, and Jiwen Lu. Tri-perspective view for vision-based 3d semantic occupancy prediction. In *CVPR*, pages 9223–9232, 2023. 7
- [11] Bu Jin, Xiaotao Hu, Yupeng Zheng, Xiaoyang Guo, Qian Zhang, Yao Yao, Diming Zhang, Xiaoxiao Long, Wei Yin, et al. Occvar: Scalable 4d occupancy prediction via next-scale prediction. *arXiv preprint arXiv:2408.14197*, 2024. 2, 6
- [12] Bernhard Kerbl, Georgios Kopanas, Thomas Leimkühler, and George Drettakis. 3d gaussian splatting for real-time radiance field rendering. *ACM Trans. Graph.*, 42(4):139–1, 2023. 2, 1
- [13] Tarasha Khurana, Peiyun Hu, David Held, and Deva Ramanan. Point cloud forecasting as a proxy for 4d occupancy forecasting. In *CVPR*, pages 1116–1124, 2023. 6
- [14] Diederik P Kingma and Max Welling. Auto-encoding variational bayes. *arXiv preprint arXiv:1312.6114*, 2013. 1, 2
- [15] Lingdong Kong, Wesley Yang, Jianbiao Mei, Youquan Liu, Ao Liang, Dekai Zhu, Dongyue Lu, Wei Yin, Xiaotao Hu, Mingkai Jia, et al. 3d and 4d world modeling: A survey. *arXiv preprint arXiv:2509.07996*, 2025. 1
- [16] Bohan Li, Jiazhe Guo, Hongsi Liu, Yingshuang Zou, Yikang Ding, Xiwu Chen, Hu Zhu, Feiyang Tan, Chi Zhang, Tiancai Wang, et al. Uniscene: Unified occupancy-centric driving scene generation. *arXiv preprint arXiv:2412.05435*, 2024. 6
- [17] Xiang Li, Pengfei Li, Yupeng Zheng, Wei Sun, Yan Wang, and Yilun Chen. Semi-supervised vision-centric 3d occupancy world model for autonomous driving. *arXiv preprint arXiv:2502.07309*, 2025. 2, 6
- [18] Zhiqi Li, Zhiding Yu, David Austin, Mingsheng Fang, Shiyi Lan, Jan Kautz, and Jose M Alvarez. Fb-occ: 3d occupancy prediction based on forward-backward view transformation. *arXiv preprint arXiv:2307.01492*, 2023. 2, 7
- [19] Zhiqi Li, Wenhai Wang, Hongyang Li, Enze Xie, Chonghao Sima, Tong Lu, Qiao Yu, and Jifeng Dai. Bevformer: learning bird’s-eye-view representation from lidar-camera via spatiotemporal transformers. *PAMI*, 2024. 4
- [20] Zhiqi Li, Zhiding Yu, Shiyi Lan, Jiahao Li, Jan Kautz, Tong Lu, and Jose M. Alvarez. Is ego status all you need for open-loop end-to-end autonomous driving? In *CVPR*, pages 14864–14873, 2024. 7
- [21] Zhimin Liao, Ping Wei, Shuaijia Chen, Haoxuan Wang, and Ziyang Ren. Stoccc: Sparse spatial-temporal cascade renovation for 3d occupancy and scene flow prediction. In *CVPR*, pages 1516–1526, 2025. 7
- [22] Zhimin Liao, Ping Wei, Ruijie Zhang, Shuaijia Chen, Haoxuan Wang, and Ziyang Ren. I²-world: Intra-inter tokenization for efficient dynamic 4d scene forecasting. *arXiv preprint arXiv:2507.09144*, 2025. 1, 2, 6, 7
- [23] Tsung-Yi Lin, Priya Goyal, Ross Girshick, Kaiming He, and Piotr Dollár. Focal loss for dense object detection. In *ICCV*, pages 2980–2988, 2017. 6
- [24] Xuewu Lin, Tianwei Lin, Zixiang Pei, Lichao Huang, and Zhizhong Su. Sparse4d: Multi-view 3d object detection with sparse spatial-temporal fusion. *arXiv preprint arXiv:2211.10581*, 2022. 3, 4
- [25] Haisong Liu, Yao Teng, Tao Lu, Haiguang Wang, and Limin Wang. Sparsebev: High-performance sparse 3d object detection from multi-camera videos. In *ICCV*, pages 18580–18590, 2023. 2, 4
- [26] Yingfei Liu, Junjie Yan, Fan Jia, Shuailin Li, Aqi Gao, Tiancai Wang, and Xiangyu Zhang. Petr2: A unified framework for 3d perception from multi-camera images. In *ICCV*, pages 3262–3272, 2023. 3
- [27] Ilya Loshchilov and Frank Hutter. Sgdr: Stochastic gradient descent with warm restarts. *arXiv preprint arXiv:1608.03983*, 2016. 7
- [28] Ilya Loshchilov and Frank Hutter. Decoupled weight decay regularization. *arXiv preprint arXiv:1711.05101*, 2017. 7
- [29] Yifan Lu, Xuanchi Ren, Jiawei Yang, Tianchang Shen, Zhangjie Wu, Jun Gao, Yue Wang, Siheng Chen, Mike Chen, Sanja Fidler, et al. Infinicube: Unbounded and controllable dynamic 3d driving scene generation with world-guided video models. *arXiv preprint arXiv:2412.03934*, 2024. 1, 8

- [30] Xuanchi Ren, Yifan Lu, Hanxue Liang, Zhangjie Wu, Huan Ling, Mike Chen, Sanja Fidler, Francis Williams, and Jiahui Huang. Scube: Instant large-scale scene reconstruction using voxplats. *NIPS*, 37:97670–97698, 2024. 8, 1
- [31] Yining Shi, Kun Jiang, Qiang Meng, Ke Wang, Jiabao Wang, Wenchao Sun, Tuopu Wen, Mengmeng Yang, and Diange Yang. Come: Adding scene-centric forecasting control to occupancy world model. *arXiv preprint arXiv:2506.13260*, 2025. 1, 2, 6, 7
- [32] Oriane Siméoni, Huy V Vo, Maximilian Seitzer, Federico Baldassarre, Maxime Oquab, Cijo Jose, Vasil Khalidov, Marc Szafraniec, Seungeun Yi, Michaël Ramamonjisoa, et al. Dinov3. *arXiv preprint arXiv:2508.10104*, 2025. 7
- [33] Wenchao Sun, Xuewu Lin, Yining Shi, Chuang Zhang, Haoran Wu, and Sifa Zheng. Sparsedrive: End-to-end autonomous driving via sparse scene representation. In *ICRA*, pages 8795–8801. IEEE, 2025. 2, 4
- [34] Pin Tang, Zhongdao Wang, Guoqing Wang, Jilai Zheng, Xiangxuan Ren, Bailan Feng, and Chao Ma. Sparseocc: Rethinking sparse latent representation for vision-based semantic occupancy prediction. In *CVPR*, pages 15035–15044, 2024. 1
- [35] Qijian Tian, Xin Tan, Yuan Xie, and Lizhuang Ma. Drivingforward: Feed-forward 3d gaussian splatting for driving scene reconstruction from flexible surround-view input. In *AAAI*, pages 7374–7382, 2025. 8, 1
- [36] Xiaoyu Tian, Tao Jiang, Longfei Yun, Yucheng Mao, Huitong Yang, Yue Wang, Yilun Wang, and Hang Zhao. Occ3d: A large-scale 3d occupancy prediction benchmark for autonomous driving. *NIPS*, 36:64318–64330, 2023. 1, 2, 6
- [37] Aaron van den Oord, Oriol Vinyals, and Koray Kavukcuoglu. Neural discrete representation learning. In *NIPS*, page 6309–6318, Red Hook, NY, USA, 2017. Curran Associates Inc. 1, 2
- [38] Jiabao Wang, Zhaojiang Liu, Qiang Meng, Liujiang Yan, Ke Wang, Jie Yang, Wei Liu, Qibin Hou, and Ming-Ming Cheng. Opus: occupancy prediction using a sparse set. *NIPS*, 37:119861–119885, 2024. 3, 6
- [39] Jianyuan Wang, Minghao Chen, Nikita Karaev, Andrea Vedaldi, Christian Rupprecht, and David Novotny. Vggt: Visual geometry grounded transformer. In *CVPR*, pages 5294–5306, 2025. 1, 2
- [40] Lening Wang, Wenzhao Zheng, Yilong Ren, Han Jiang, Zhiyong Cui, Haiyang Yu, and Jiwen Lu. Occsora: 4d occupancy generation models as world simulators for autonomous driving. *arXiv preprint arXiv:2405.20337*, 2024. 1, 2
- [41] Shihao Wang, Yingfei Liu, Tiancai Wang, Ying Li, and Xiangyu Zhang. Exploring object-centric temporal modeling for efficient multi-view 3d object detection. In *ICCV*, pages 3621–3631, 2023. 4
- [42] Yue Wang, Vitor Campagnolo Guizilini, Tianyuan Zhang, Yilun Wang, Hang Zhao, and Justin Solomon. Detr3d: 3d object detection from multi-view images via 3d-to-2d queries. In *CoRL*, pages 180–191. PMLR, 2022. 4
- [43] Yuping Wang, Xiangyu Huang, Xiaokang Sun, Mingxuan Yan, Shuo Xing, Zhengzhong Tu, and Jiachen Li. Uniocc: A unified benchmark for occupancy forecasting and prediction in autonomous driving. *arXiv preprint arXiv:2503.24381*, 2025. 1
- [44] Julong Wei, Shanshuai Yuan, Pengfei Li, Qingda Hu, Zhongxue Gan, and Wenchao Ding. Occllama: An occupancy-language-action generative world model for autonomous driving. *arXiv preprint arXiv:2409.03272*, 2024. 2, 6
- [45] Haoran Xu, Peixi Peng, Guang Tan, Yiqian Chang, Yisen Zhao, and Yonghong Tian. Delta-triplane transformers as occupancy world models. *arXiv preprint arXiv:2503.07338*, 2025. 2, 6
- [46] Jingyi Xu, Xieyuanli Chen, Junyi Ma, Jiawei Huang, Jintao Xu, Yue Wang, and Ling Pei. Spatiotemporal decoupling for efficient vision-based occupancy forecasting. In *CVPR*, pages 22338–22347, 2025. 2
- [47] Tianshuo Xu, Hao Lu, Xu Yan, Yingjie Cai, Bingbing Liu, and Yingcong Chen. Occ-llm: Enhancing autonomous driving with occupancy-based large language models. *arXiv preprint arXiv:2502.06419*, 2025. 1, 2, 6
- [48] Ziyang Yan, Wenzhen Dong, Yihua Shao, Yuhang Lu, Liu Haiyang, Jingwen Liu, Haozhe Wang, Zhe Wang, Yan Wang, Fabio Remondino, et al. Renderworld: World model with self-supervised 3d label. *arXiv preprint arXiv:2409.11356*, 2024. 2, 6
- [49] Yu Yang, Jianbiao Mei, Yukai Ma, Siliang Du, Wenqing Chen, Yijie Qian, Yuxiang Feng, and Yong Liu. Driving in the occupancy world: Vision-centric 4d occupancy forecasting and planning via world models for autonomous driving. In *AAAI*, pages 9327–9335, 2025. 2
- [50] Zetong Yang, Li Chen, Yanan Sun, and Hongyang Li. Visual point cloud forecasting enables scalable autonomous driving. In *CVPR*, pages 14673–14684, 2024. 6
- [51] Haiming Zhang, Ying Xue, Xu Yan, Jiacheng Zhang, Weichao Qiu, Dongfeng Bai, Bingbing Liu, Shuguang Cui, and Zhen Li. An efficient occupancy world model via decoupled dynamic flow and image-assisted training. *arXiv preprint arXiv:2412.13772*, 2024. 1, 2, 6, 7
- [52] Lvmin Zhang, Anyi Rao, and Maneesh Agrawala. Adding conditional control to text-to-image diffusion models. In *ICCV*, pages 3836–3847, 2023. 2
- [53] Wenzhao Zheng, Weiliang Chen, Yuanhui Huang, Borui Zhang, Yueqi Duan, and Jiwen Lu. Occworld: Learning a 3d occupancy world model for autonomous driving. In *ECCV*, pages 55–72. Springer, 2024. 1, 2, 6, 7
- [54] Wenzhao Zheng, Junjie Wu, Yao Zheng, Sicheng Zuo, Zixun Xie, Longchao Yang, Yong Pan, Zhihui Hao, Peng Jia, Xi'anpeng Lang, et al. Gaussianad: Gaussian-centric end-to-end autonomous driving. *arXiv preprint arXiv:2412.10371*, 2024. 2

SparseWorld-TC: Trajectory-Conditioned Sparse Occupancy World Model

Supplementary Material

A. Additional Quantitative Experiments

A.1. Ray-level mIoU

SparseOcc [34] proposes RayIoU (Ray-level mIoU) to solve the inconsistency penalty along the depth axis raised in traditional voxel-level mIoU criteria. We evaluate our SparseWorld-TC-Large* model with this ray-level metric and report the results in Table 5.

Table 5. RayIoU scores [%] of 4D occupancy forecasting performance on the Occ3D-nuScenes [36] benchmark.

	RayIoU _{1m}	RayIoU _{2m}	RayIoU _{4m}	RayIoU
Recon.	35.4	43.0	47.8	42.1
1s	29.5	36.5	41.4	35.8
2s	25.8	32.1	36.8	31.6
3s	23.5	29.4	33.8	28.9

A.2. Ablation study on trajectory embedding

We further explore the influence of embedding modules for the trajectory condition. The modules named “TE”, “PE” and “STE” represent time embedding, position embedding and spatiotemporal embedding, respectively. The performance of our SparseWorld-TC-Small model in different settings is summarized in Table 6.

Table 6. Ablation study on embedding modules. Avg. denotes average performance of mIoU or IoU in 1s, 2s, and 3s.

Modules			mIoU (%) ↑	IoU (%) ↑
TE	PE	STE	Avg.	Avg.
			15.44	32.19
✓			17.45	35.06
✓	✓		23.07	47.53
✓	✓	✓	25.60	49.02

A.3. Per-class performance

As shown in Table 7 and Table 8, we report the performance per-class of our SparseWorld-TC-Large* (Ours-Large* for short). Our approach not only maintains the geometric consistency of static scenes, but also predicts the dynamic objects relatively accurately.

B. Additional Qualitative Experiments

B.1. Feedforward Gaussian

Inspired by advances in feedforward Gaussian methods [29, 30, 35], we extend the original model with additional MLPs to decode Gaussian parameters from latent features. Then we utilize the differential Gaussian rasterization proposed in 3DGS [12] to render the predicted front-view image and calculate L1 loss with the GT image.

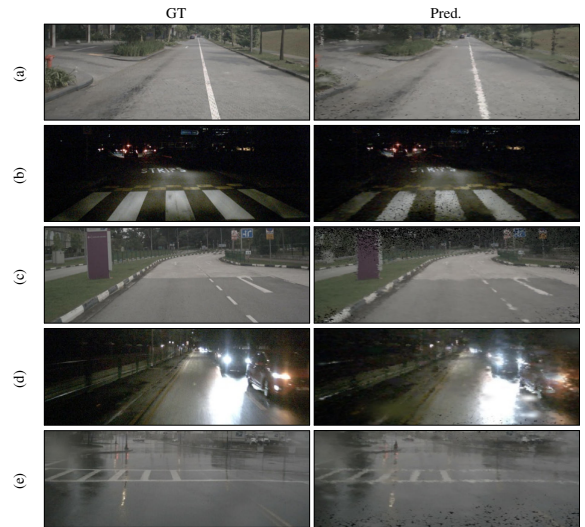


Figure 7. Gaussian splatting reconstruction during training.

The reconstruction and future forecasting of sensor observation, as shown Figure 7 and Figure 8, demonstrate the potential of our model in leveraging the Gaussian representation and achieving self-supervised training in the future.



Figure 8. Future observation forecasting on validation set.

B.2. Additional Trajectory-conditioned Prediction

More visualizations are shown below.

Table 7. Per-class mIoU [%] performance of 4D occupancy forecasting on Occ3D-nuScenes [36].

Ours-Large*	mIoU	IoU	others	barrier	bicycle	bus	car	const. veh.	motorcycle	pedestrian	traffic cone	trailer	truck	drive. suf.	other flat	sidewalk	terrain	manmade	vegetation
Recon.	37.92	57.65	13.15	45.06	26.72	40.26	46.44	24.62	25.38	21.47	28.99	34.84	35.92	76.87	44.76	51.14	49.71	40.98	38.38
1s	32.76	55.28	12.25	42.04	19.22	29.07	32.03	22.42	15.70	10.28	24.24	30.55	27.37	74.98	43.12	49.53	48.43	39.03	36.68
2s	29.62	53.56	11.40	38.75	15.61	20.72	25.49	19.93	13.46	6.01	19.55	26.27	22.35	74.46	42.20	48.34	47.42	36.82	34.76
3s	27.28	51.71	10.36	35.19	12.38	16.90	22.22	17.73	11.75	4.29	15.14	23.78	20.04	73.56	40.62	46.71	45.89	34.49	32.66

Table 8. Per-class RayIoU [%] performance of 4D occupancy forecasting on Occ3D-nuScenes [36].

Ours-Large*	RayIoU	others	barrier	bicycle	bus	car	const. veh.	motorcycle	pedestrian	traffic cone	trailer	truck	drive. suf.	other flat	sidewalk	terrain	manmade	vegetation
Recon.	42.1	11.7	47.3	31.7	63.6	56.3	28.7	30.4	35.2	32.3	37.1	52.4	70.4	40.7	38.1	40.2	53.1	46.2
1s	35.8	10.5	44.8	19.8	47.2	43.0	26.7	17.6	21.6	29.1	31.0	44.5	66.0	37.9	35.5	38.3	50.8	44.2
2s	31.6	9.7	41.9	15.9	34.4	34.1	25.1	15.1	13.7	25.8	21.9	39.7	62.8	36.1	33.6	36.7	48.3	41.8
3s	28.9	9.0	39.3	12.9	28.5	29.9	23.9	13.5	10.1	22.5	19.1	36.7	60.2	34.1	31.8	34.8	45.8	39.3

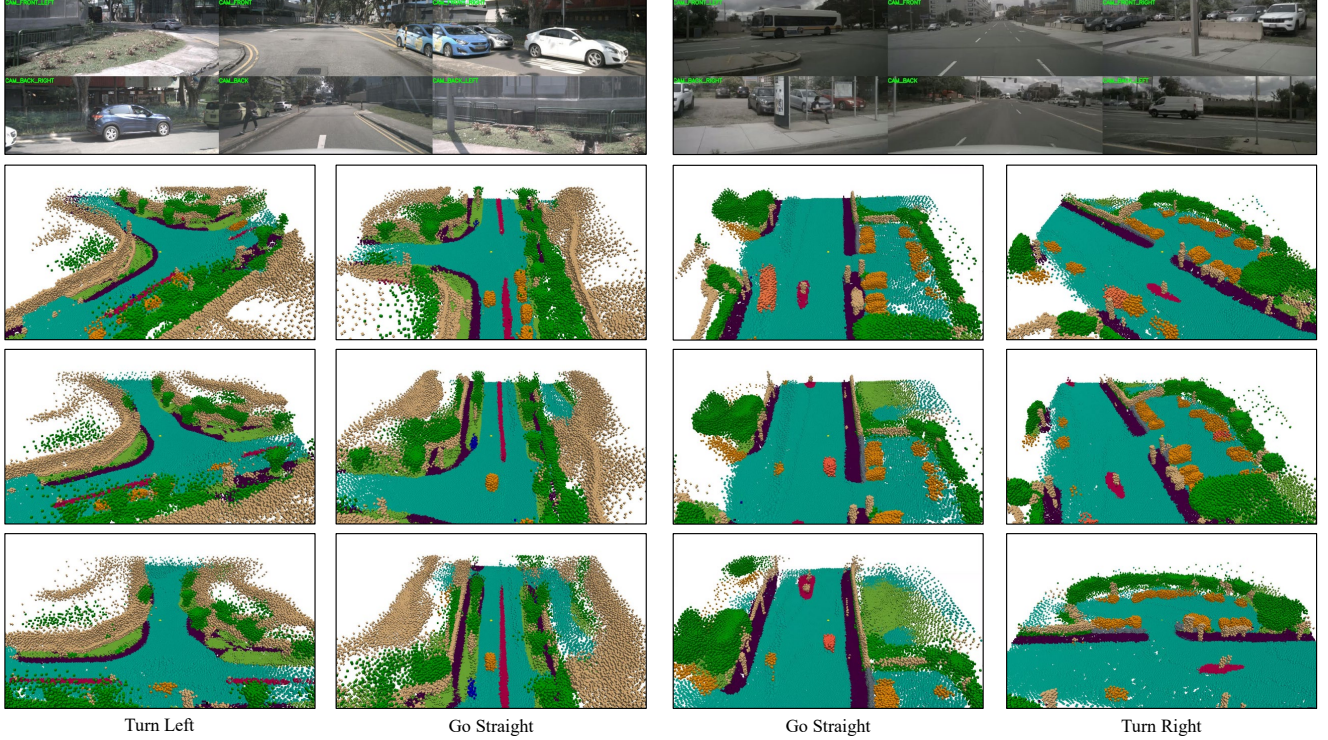


Figure 9. Additional qualitative results in the different trajectory conditions.

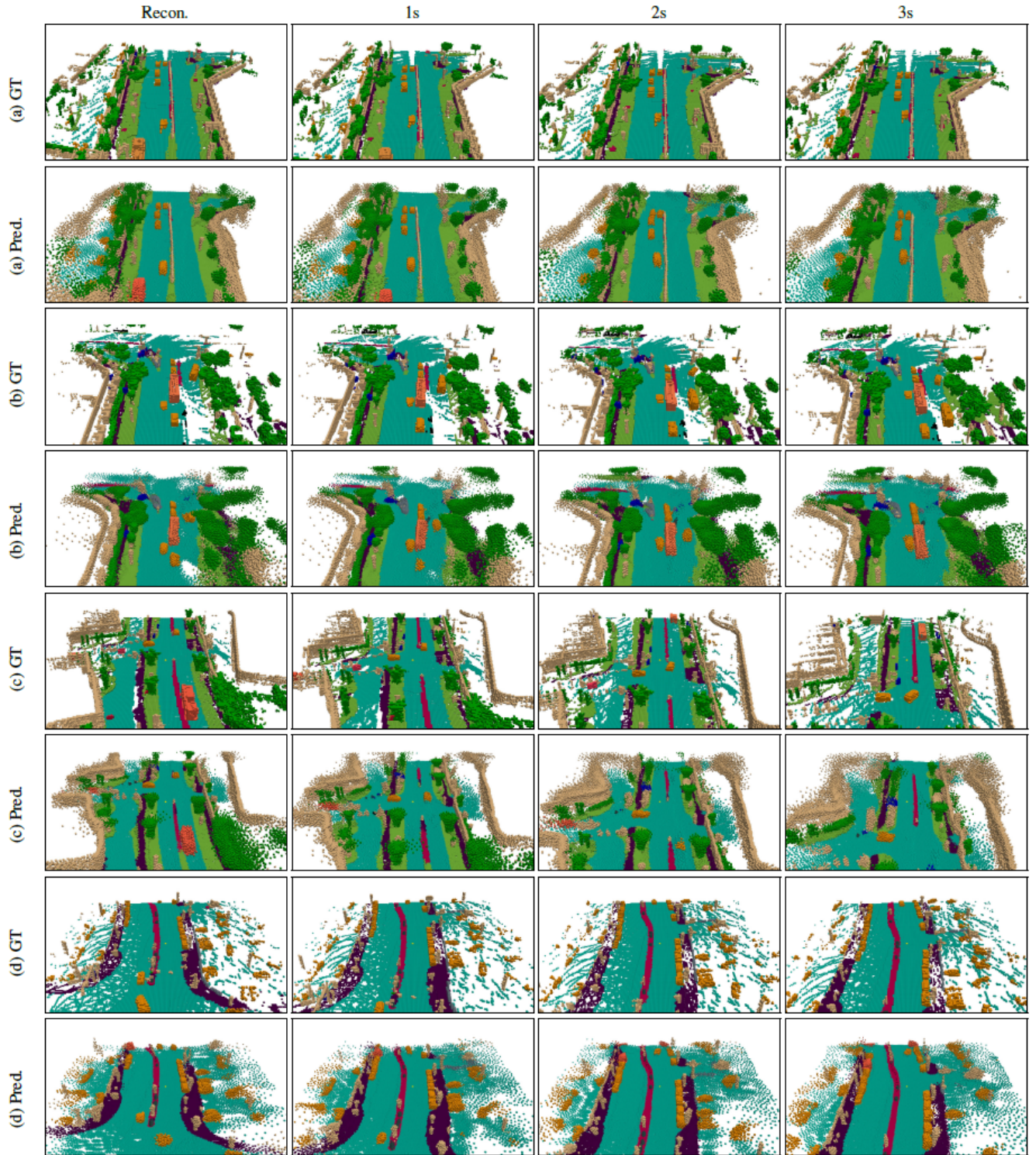


Figure 10. Additional qualitative results of our proposed SparseWorld-TC are presented here.

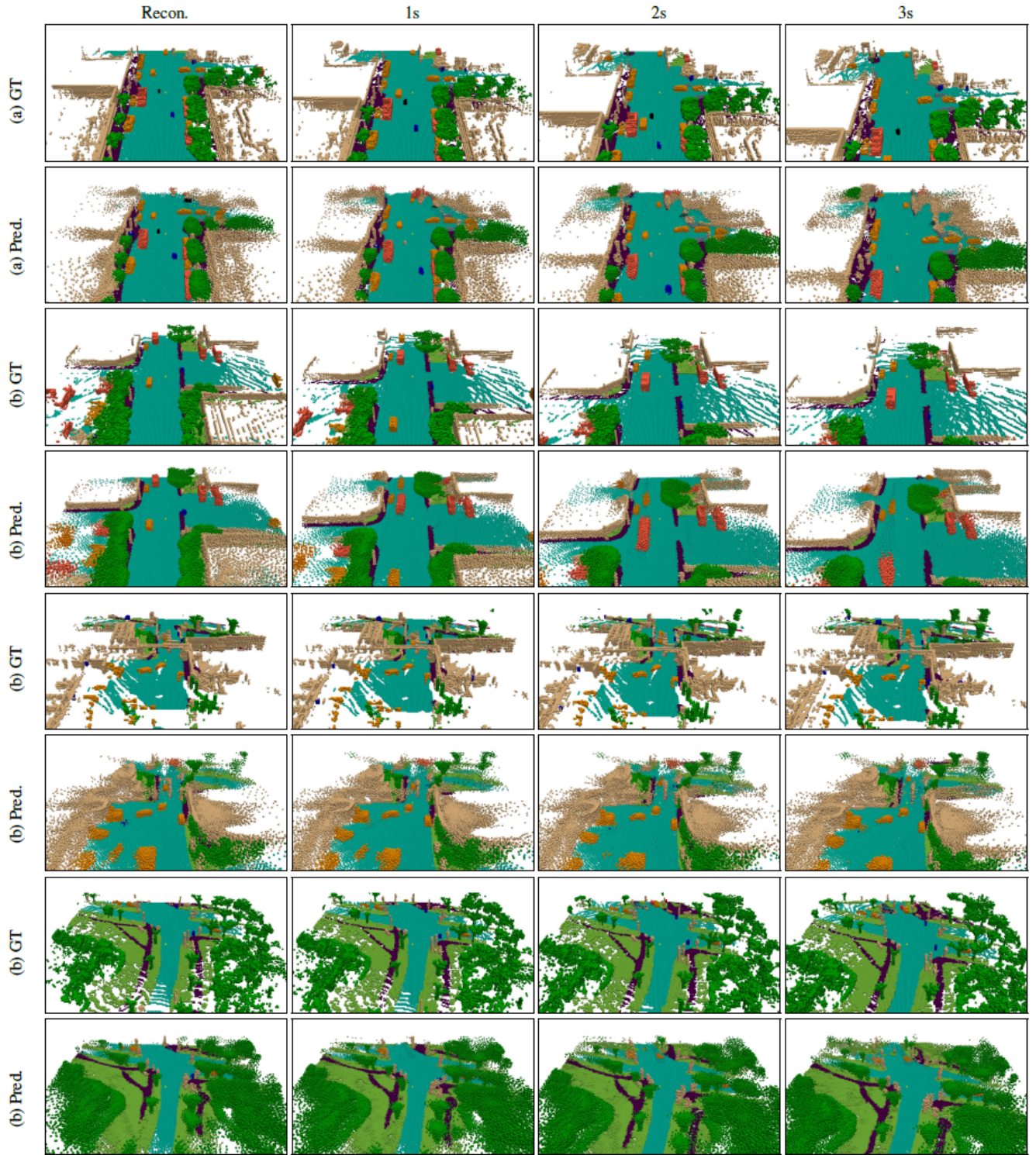


Figure 11. Additional qualitative results of our proposed SparseWorld-TC are presented here.